Contribution of topology determinants of a viral movement protein to its membrane association, intracellular traffic and viral cell-to-cell movement

A. Genovés[1], V. Pallás*, and J. A. Navarro

Instituto de Biología Molecular y Celular de Plantas, IBMCP (Universitat Politècnica de València-Consejo Superior de Investigaciones Científicas) Avenida Ingeniero Fausto Elio, s/n, 46022, Valencia, Spain.

[1]Present address: Centro de Investigación Príncipe Felipe, Avenida Autopista del Saler, 16, E-46013, Valencia, Spain.

Abstract word count: 242

Text word count: 6722

Running title: MNSV p7B topology determinants-function relationship

Corresponding author address:

Dr. Vicente Pallás

Instituto de Biología Molecular y Celular de Plantas (IBMCP). UPV-CSIC, Avenida Ingeniero Fausto Elio, s/n, 46022, Valencia, Spain.

Telephone: 34 963877877, FAX: 34 963877859, e-mail: vpallas@ibmcp.upv.es

ABSTRACT

The p7B movement protein (MP) of *Melon necrotic spot virus* (MNSV) is a single-pass membrane protein associated with the endoplasmic reticulum (ER), the Golgi apparatus (GA) and plasmodesmata (Pd). Experimental data presented here revealed that the p7B transmembrane domain (TMD) was sufficient to target the green fluorescent protein (GFP) to ER membranes. In addition, the short extramembrane regions of p7B were essential for subsequent ER export and transport to GA and Pd. Microsomal partitioning and bimolecular fluorescence assays supported a type II topology of p7B in planta. Mutations affecting conventional determinants of p7B membrane topology such as TMD secondary structure, overall hydrophobicity profile, the so-called “aromatic belt” and the net charge distribution on either side of the TMD were engineered into infectious RNAs to investigate the relationship between the MP structure and MNSV cell-to-cell movement. Results revealed that: i) the overall hydrophobic profile and the α-helix integrity of the TMD were relevant for virus movement; ii) modification of the net charge balance of the regions flanking both TMD sides drastically reduced cell-to-cell movement; iii) localization of p7B to GA was necessary but not sufficient for virus movement and iv) membrane insertion was essential for p7B function in virus movement. Our results therefore indicate that MNSV cell-to-cell movement requires a sequential transport of p7B from the ER via the GA to Pd, which is modulated by a combination of several signals with different strengths in the extramembrane regions and TMD of the MP.

INTRODUCTION

The association of plant positive-strand RNA viruses with plant cell endomembranes is a critical event that occurs during the virus life cycle. Many viral factors are proteins containing hydrophobic regions that, generally, induce drastic modifications in endoplasmic reticulum (ER) morphology, nuclear envelope and others membrane-bound organelles. These cytopathic rearrangements either result in the formation of membrane-associated invaginations, free cytoplasmic vesicles or multivesicular bodies that provide protective environments and enlarged surfaces for not only genome replication, translation and particle assembly but also for intracellular and cell-to-cell movement (1, 33, 39, 53).

How plant viruses take advantage of the intracellular endomembrane system to move appears related to the structural characteristics of one or more virus-encoded movement proteins (MPs) (37, 52, 55). For example, *Tobacco mosaic virus* (TMV) MP is a tightly associated membrane protein that was proposed to contain two helical hydrophobic domains spanning the ER membrane (8, 16). TMV MP together with TMV 126-kDa protein, which respectively have movement and replication functions, cause a transient aggregation of the ER resulting in the formation of cytoplasmic membrane bodies where TMV replicates (viral replication complexes, VRCs) (23, 31). These viral factories travel toward the cell host periphery in a cytoskeleton-dependent manner, resulting in entry into neighboring cells by traversing the cell wall through the plasmodesmata (Pd) (24, 48). MP association with ER membranes has also been described for viruses whose MPs induce tubule formation in Pd. For example, *Alfalfa mosaic virus* (AMV) MP behaves as an integral membrane protein and localizes to the ER (29). In addition, *Prunus necrotic ringspot virus* (PNRSV) MP has one hydrophobic region that mediates its association with biological membranes. However, this region is not thought to traverse the entire lipid bilayer, but rather is embedded in the

membrane interface with the N and C termini oriented toward the cytoplasm (41). The intracellular transport and cell-to-cell movement of some flexible rod viruses belonging to nine different genera are driven by the triple gene block of movement proteins (TGBp1, TGBp2 and TGBp3). TGBp1s are multifunctional RNA-binding proteins. All TGBp2s contain two transmembrane domains (TMD) whereas TGBp3s form two main groups having either one (potex-like group) or two (hordei-like group) TMDs. Several groups have reported that the interactions among the three components of the TGB module might differ depending on virus genera, with four models recently proposed to summarize the collective findings (57). Regardless of the interaction model and virus, TGB2 and TGB3 proteins are always associated with ER membranes and, occasionally, with ER-derived vesicles which move along the actin network to reach the Pd (57).

Association of viral MPs with plant endomembranes has also been reported for p6 of *Beet yellows virus* (BYV) and for p7B of *Melon necrotic spot virus* (MNSV) (20, 44). Both proteins contain a very hydrophobic TMD that inserts into the ER membrane. Interestingly, the most important difference between these MPs is that p7B moves from ER to Golgi apparatus (GA), followed by targeting to Pd (20) while BYV p6 remains in the ER membrane (44). The ER-GA-Pd pathway described for p7B migration has also been observed for cellular proteins such as the class 1 reversibly glycosylated polypeptides and the family of plasmodesmata-located proteins (PDLP1) (49, 56).

The MNSV p7B is one of the two small MPs encoded by carmoviruses that are essential for virus cell-to-cell movement (18). By using *in vitro* translation assays in the presence of canine pancreas rough microsomes, it was recently demonstrated that membrane association of p7B requires its TMD (42). Moreover, as occurs for most integral membrane proteins, the p7B TMD adopts an α-helix conformation that is co-translationally inserted into the lipidic

bilayer through the ER translocon (40). The translocation machineries play a central role in helix-bundle membrane protein topology controlling TMD insertion and orientation into lipid bilayers (25). Total hydrophobicity and helix arrangement of the TMD together with the distribution of aromatic and charged amino acids on either side of the hydrophobic region are critical features that affect TMD-lipid bilayer interaction and, consequently, TMD recognition in the ribosome-translocon channel (27, 34, 59, 60).

While viral MPs have been shown to interact with biological membranes, our knowledge about the role of MP membrane topology in MP transport to Pd and in viral cell-to-cell movement has been largely restricted to TMV-like MPs and the TGB system (28, 57). Therefore, extending these studies to other viruses with different types of MPs should allow a better understanding of virus-plant interactions. For this report, we investigated whether membrane association, intracellular transport of p7B and MNSV cell-to-cell movement were influenced by altering topological determinants of the MP.

MATERIALS AND METHODS

Construction of binary vectors for p7B membrane topology studies and site-directed mutagenesis. MNSV p7B ORF was PCR-amplified from plasmid pMNSV(Al) (accession number DQ339157) (18). Amino-terminal and carboxy-terminal fusions of MNSV p7B to the N-terminal fragment (residues 1-155) of the yellow fluorescent protein (p7B-N_t[YFP] and N_t[YFP]-p7B, respectively) were cloned into binary vector pMOG 800 between the CaMV 35S promoter and the potato proteinase inhibitor II terminator (PoPit) (32). CaMV 35S expression cassettes corresponding either to the ER-targeted N_t[YFP] (ER-N_t[YFP]) or to the ER-targeted C-terminal fragment (residues 156-238) of the YFP (ER-C_t[YFP]) were obtained by HindIII-digestion of pRT-YN-ER and pRT-YC-ER, respectively (62), and then cloned into HindIII-linearized pMOG800. pRT-YN-ER and pRT-YC-ER plasmids were kindly provided by Dr Jari

P. T. Valkonen. Binary vectors expressing either N_t[YFP] or C_t[YFP] cytosolic fragments were previously described (3).

Site-direct mutations were introduced into the p7B open reading frame (ORF) of the pMNSV(Al)-Δcp-GFP clone from which infectious RNAs expressing the green fluorescent protein (GFP) can be obtained (18, 19). For subcellular localization in *N. benthamiana*, mutations were incorporated into the previously described binary vector expressing GFP-p7B (20). For membrane orientation studies in *N. benthamiana*, several mutations were introduced into binary vectors expressing either p7B-N_t[YFP] or N_t[YFP]-p7B. QuickChangeR XL-Site Direct Mutagenesis Kit (Stratagene, La Jolla, California) and the primer pairs enumerated in supplemental Table S1 were used.

***In vitro* transcription and plant inoculation.** Viral cell-to-cell movement was assayed as previously described (18, 19). Briefly, infectious RNAs were obtained from pMNSV(Al)-Δcp-GFP clones containing either the wild-type p7B or each mutant variant ORF (see supplemental Table S1). Transcripts were inoculated in *Cucumis melo* (cv. Galia) cotyledons transiently expressing MNSV coat protein (p42) (18, 19). At least, three independent bioassays with five plants per each mutant RNA were performed. At three days post-inoculation (dpi), 20-30 images of individual fluorescent infection foci were taken with a confocal microscope (Leica TCS SL, Leica Microsystems GmbH, Wetzlar, Germany). Fluorescent infection areas were measured using ImageJ 1.41o software and data analyzed with MS Excel.

***Agrobacterium tumefaciens*-mediated transient expression and bimolecular fluorescence complementation assays**. Transient expression assays on *N. benthamiana* plants were performed as previously described (18). Briefly, the binary constructs were

137 introduced into the *Agrobacterium tumefaciens* strain C58C1 by electroporation (GenePulser
138 XcellTM electroporation system, Bio-Rad Laboratories, Hercules, California). Transformed
139 bacteria were grown overnight in a shaking incubator at 28ºC in Luria-Bertani (LB) medium
140 supplemented with the appropriate antibiotic mixture. Cultures were collected by slow-speed
141 centrifugation and adjusted to the required final OD600 value (0.2) with 10 mM $MgCl_2$, 10 mM
142 MES pH 5.6 and 150 μM acetosyringone. These suspensions were infiltrated into two-week-
143 old *N. benthamiana* plants by gentle pressure infiltration into the lower side of the leaves. For
144 co-localization and bimolecular fluorescence complementation experiments requiring the
145 simultaneous expression of two or more different proteins, individual bacterial cultures
146 containing the corresponding binary vectors were adjusted to a final OD600 of 0.2 and mixed
147 before leaf infiltration. Moreover, a gene silencing suppressor (HC-Pro) was added in BiFC
148 assays as reported (62). Plants were kept in growth chambers in 16h light at 25ºC and 8h
149 dark at 22ºC.

150 **Membrane partitioning and immunoblotting analysis.** Approximately 2 g of *N.*
151 *benthamiana* leaves transiently expressing either GFP-p7B or each mutant protein were
152 homogenized in lysis buffer containing 20 mM HEPES, pH 6.8; 150 mM potassium acetate;
153 250 mM mannitol and 1 mM $MgCl_2$. Large cellular debris was removed by gentle
154 centrifugation at 3000 X *g* for 10 min, and the resulting supernatant was ultracentrifuged at
155 30000 X *g* for 1 h to generate the soluble (S30) and the microsomal (P30) fractions. For
156 chemical treatments, microsomal pellets were resuspended in 10 vol of 100 mM Na_2CO_3 (pH
157 11), 4 M urea, lysis buffer containing 1% Triton X-100 or original lysis buffer. After incubation
158 for 30 min on ice the samples were centrifuged at 30000 X *g* for 1 h. The resulting pellet was
159 resuspended in lysis buffer. All fractions were analyzed by SDS-PAGE in 12% polyacrylamide
160 gels, and subsequently transferred to polyvinylidene fluoride membranes (PVDF) (GE

161 Healthcare, Buckinghamshire, England) for immunoblotting with anti-GFP mouse polyclonal
162 antibody (Roche Diagnostics GmbH, Mannheim, Germany).

163 **Confocal laser scanning microscopy.** *N. benthamiana* leaf tissue was mounted in water
164 under a coverslip between 36 and 48 h following infiltration with *Agrobacterium* containing the
165 required constructs. All imaging was conducted with a Leica TCS SL confocal laser-scanning
166 microscope using an HCX APO 40x/0.90 w water dipping lens to study the subcellular
167 localization of the fluorescent tagged proteins. eGFP and YFP fluorescence was visualized by
168 488 nm excitation with a Kr/Ar laser and their emission was examined with a bandpass filter
169 for 500-530 nm. For imaging of ChFP and mRFP fluorescence, excitation at 514 nm (He/Ne
170 laser) was used whereas the emission was observed at 600-620 (ChFP) and 550-590 nm
171 (mRFP). Sequential scanning was used to suppress optical cross-talk between the
172 fluorophores in stationary structures colocalization assays. However, for dynamic structures,
173 simultaneous scanning was employed to avoid green and red color misalignment.

174 **Computer-assisted analysis of secondary structure and transmembrane helices.**
175 Prediction of transmembrane helices of MNSV p7B and mutant sequences was performed
176 with Membrane Protein Explorer (MPEx) software version 3.0
177 (http://blanco.biomol.uci.edu/mpex/). Free energy profile for membrane insertion of
178 hydrophobic transmembrane proteins was estimated with ΔG Prediction Server v1.0
179 (http://www.cbr.su.se/DGpred/). Secondary structure prediction of proteins was performed
180 with SSPro 2.01 software (SYMPRED server, http://www.ibi.vu.nl/programs/sympredwww/).

181 **RESULTS**

182 **Structural characteristics of the MNSV p7B hydrophobic domain.**

183 MNSV p7B is a single-pass membrane protein that inserts co-translationally into the
184 membrane of canine ER microsomes following a translocon-mediated pathway (40, 42).

185 Depending on the computer-based method used, the p7B TMD length oscillates from 18 to 23
186 residues (data not shown) although all predictions share a consensus hydrophobic core from
187 Y13 to L32 that mainly contains hydrophobic residues (A, I, V, L and F) (Fig. 1A). The
188 theoretical value calculated for the apparent free energy of the p7B TMD was negative
189 enough (ΔG_{app} = -1.869 kcal mol^{-1}) to be efficiently integrated into the ER membrane (25, 27)
190 as previously reported (40).

191 Residues distribution and conformational preferences of the lateral chains determine the
192 precise positioning of transmembrane helices in cellular membranes. Residues such as
193 lysine, arginine, tryptophan and tyrosine in membrane-buried helices often extend their side
194 chain perpendicularly to the membrane bilayer and point away from the hydrophobic core
195 generating a snorkeling effect (11). According to these observations, the side chain of the Y28
196 residue is expected to snorkel out of the p7B TMD hydrophobic core. In addition, analyses of
197 TMDs from numerous membrane proteins have revealed that aromatic residues, in particular
198 tyrosine, have a propensity to mainly locate at or near the lipid-water interface of the
199 membrane (22, 35, 43). Therefore, the Y13 residue may reside at the p7B TMD helix end
200 where it favorably interacts with cellular environment. Aromatic residues in this position have
201 been referred to as “aromatic belts”. Their functional significance is not known, although it has
202 been speculated that aromatic belts perform an important function in membrane anchoring
203 and stabilization of the corresponding protein (25). Finally, turn-promoting proline residues are
204 excluded from the p7B TMD (26, 58).

205 **Assessment of the MNSV p7B topology in plant ER membranes.**

206 To study the integration of p7B in plant cell ER membranes, the p7B TMD (Y13-L32) was
207 cloned as a carboxy-terminal fusion to the green fluorescent protein (GFP-tmd(p7B)) (Fig. 1A)
208 and transiently expressed by agroinfiltration in *N. benthamiana* leaves. At 48 h post infiltration,

GFP-tmd(p7B) fluorescence appeared as an elaborate polygonal network (Fig. 1B) very reminiscent to that observed with mGFP5-KDEL, a luminal ER marker (Fig. 1C). Remarkably, GFP-tmd(p7B) was retained in the ER while GFP-p7B was fully exported from the ER and located at cytoplasmic granules (Fig. 1D) which colocalized with Golgi stacks (Fig. 1E) (20). STtmdChFP, a Golgi-specific reporter consisting in the transmembrane domain of the rat α-2,6-sialyltransferase fused to the cherry fluorescent protein was used for this co-localization assay. Images here and elsewhere in the report, are representative of those observed in at least three independent experiments.

We also analyzed the association of GFP-tmd(p7B) with cellular membranes by subcellular fractionation. *N. benthamiana* tissue expressing GFP-tmd(p7B) was lysed and extracts were separated by high-speed centrifugation into pellet (P30) and supernatant (S30) fractions. The P30 fraction was resuspended and divided into several aliquots which were extracted with either 0.1M Na_2CO_3 (pH 11) which would dislodge proteins entrapped within membrane structures, 4M urea which would dislodge proteins peripherically bound to the membrane or extracted with Triton X-100 which would release integral membrane proteins. Control experiments were performed including GFP-p7B fusion and *Beet yellows virus* p6 fused to GFP (GFP-p6) (20, 44). GFP-tmd(p7B), as well as GFP-p7B and GFP-p6 control proteins behaved like typical integral membrane proteins because all of them were extracted from the membrane fraction only after incubation with Triton X-100 (Fig. 1F).

In vitro and *in vivo* assays using canine microsomal membranes and prokaryotic cells (*Escherichia coli*), respectively, revealed that p7B integrates into the ER membrane with an N_{cyt}-C_{lum} orientation (40). Since it has been shown that topological determinants of membrane proteins are affected by lipid composition of host membranes, which can differ among animal microsomes, the prokaryotic inner-membrane, and the ER membrane of plant cells (14), we

studied *in vivo* the p7B membrane orientation in the plant ER. We employed a novel bimolecular fluorescence complementation (BiFC) based assay previously described for topology studies of both BYV p6 and *Potato mop-top virus*-encoded integral membrane TGBp2 (62). This technique relies on the formation of a fluorescent complex between a fragment of the yellow fluorescent protein (YFP) targeted either to the cytoplasm or to the ER luminal space and a counterpart fragment fused to the integral membrane protein N- or C-terminus. When overexpressed, the two YFP halves interact and therefore yield a fluorescent YFP, if they are located in the same subcellular compartment (62).

Amino-terminal and carboxy-terminal fusions of p7B to the N-terminal YFP fragment (p7B-N_t[YFP] and N_t[YFP]-p7B, respectively) were transiently coexpressed with the complementary C-terminal half of YFP, targeted either to the cytosol (C_t[YFP]) or to the ER lumen (ER-C_t[YFP]). Confocal microscopy analysis revealed that p7B-N_t[YFP] expression in the presence of either C_t[YFP] or ER-C_t[YFP] only restored fluorescence, which clearly highlighted the ER network, in the latter combination (Fig. 1G and 1H, respectively). According to single-pass membrane status of p7B, the fluorescence was also observed when N_t[YFP]-p7B and C_t[YFP] were expressed together (Fig. 1I). No fluorescence was visible for the N_t[YFP]-p7B and ER-C_t[YFP] combination (Fig. 1J). After the coexpression of N_t[YFP] and C_t[YFP], fluorescence was observed in the cytoplasm and nuclei (Fig. 1K) indicating that expression level of each split YFP-fragment was sufficient to allow fluorescence complementation (62). Alternatively, fluorescence was confined to the ER network after the coexpression of ER-N_t[YFP] and ER-C_t[YFP] (Fig. 1L) indicating that both proteins were properly targeted to the ER lumen (62). The coexpression of either N_t[YFP] and ER-C_t[YFP] or the ER-N_t[YFP] and C_t[YFP] combination resulted in no fluorescence detection indicating that each YFP-split fragment was fully located in the appropriate subcellular compartment (Fig. 1M and 1N, respectively). Taken

257 together our observations indicate that in plant cells, as occurs in heterologous systems, the
258 N-terminal region of p7B (residues 1-12) is exposed to the cytoplasm whereas the C-terminal
259 domain (residues 33-60) faces the ER luminal side (type II topology).

260 **Contribution of the p7B topology determinants to MNSV cell-to-cell movement.**

261 To assess the relevance of p7B topology determinants in MNSV cell-to-cell movement, a
262 series of site-directed mutations was introduced into the p7B ORF of the pMNSV(Al)-Δcp-GFP
263 clone (Fig. 2A) from which infectious transcripts expressing free GFP can be obtained (18).
264 Wild-type (Fig. 2B) and mutant (Fig. 2C to 2U and Table 1) MNSV RNAs were inoculated in
265 cotyledons of melon plants and local spread of infection was measured by quantifying the
266 fluorescent area. The results are presented according to the p7B topological determinant
267 affected.

268 *Mutations affecting p7B TMD hydrophobicity.* Since the most prominent p7B topological
269 determinant is the Y13-L32 hydrophobic region (30, 61), different mutations were directed to
270 modify TMD hydrophobicity. Amino acid replacement strategy was used instead of amino acid
271 deletion/insertion to preserve the p7B TMD length (Table S2) because the distribution of
272 single-pass membrane proteins along the organelles of the secretory pathway depends on
273 their TMD length (7). Hydrophobicity was reduced by engineering different alanine
274 replacements (A-replacement) of hydrophobic V, L and I as well as of aromatic F and Y
275 residues which were positioned between residues S14 and L32 (5). A-replacements, which
276 were initially made in groups of three, led to a 0.6-4 fold reduction of wild-type TMD
277 hydrophobicity (Table 1). TMD hydrophobicity of each mutant was measured as free energy
278 for membrane insertion using the “biological” scale determined by Hessa et al. (25). Upon
279 inoculation, all the triple mutants were completely arrested to single, initially infected cells (Fig
280 2C to 2F and Table 1).

281 Considering that a hydrophobicity threshold is required for accurate integration of TMDs,
282 we evaluated the relationship of this phenomenon with MNSV cell-to-cell movement. For this
283 purpose, p7B TMD hydrophobicity was progressively reduced by introducing double or single
284 A-replacements into the S14-L32 hydrophobic region. All mutants showing TMD free energies
285 higher than -1.191 kcal mol^{-1} (obtained with the $F_{27}AI_{29}A$ mutant, Fig. 2G and Table 1) were
286 competent in cell-to-cell movement although the infected area slightly reduced (Fig. 2H to 2J
287 and Table 1) compared with wild-type RNA cell-to-cell movement (Fig 2B). To segregate the
288 putative adverse effect in the cell-to-cell movement generated by introducing multiple
289 mutations into p7B TMD from that produced by the TMD hydrophobicity reduction itself,
290 another p7B mutant was obtained in which positions 22 through to 25 were replaced with
291 alanines (the $I_{22}AS_{23}AF_{24}AV_{25}A$ mutant). The resulting ΔG_{app} was similar to that obtained with
292 the $L_{18}A$ mutant (-1.465 kcal mol^{-1} vs -1.472 kcal mol^{-1}, respectively). Interestingly, this mutant
293 was functional in viral cell-to-cell movement (81% of the local movement in relation to the
294 wild-type RNA, Fig. 2K and Table 1).
295 In addition, the effect of increasing p7B TMD hydrophobicity in cell-to-cell movement was
296 also assessed. For this purpose, positions 24 through to 26 were altered to leucines instead
297 of to alanines (the $F_{24}LV_{25}LF_{26}L$ mutant) to slightly increment TMD hydrophobicity
298 (ΔG_{app} (3L) = -2.383 vs ΔG_{app}(wt) = -1.869 kcal mol^{-1}) (Table 1). In contrast to the
299 $F_{24}AV_{25}AF_{26}A$ mutant, this modification apparently had no effect on cell-to-cell movement (Fig.
300 2L and Table 1). However, a 2-fold increment of TMD hydrophobicity, which was obtained by
301 replacing positions 22 through to 25 with leucines (ΔG_{app} (4L) = -3.630 vs
302 ΔG_{app}(wt) = -1.869 kcal mol^{-1}), drastically reduced viral movement (9.7%) (Fig. 2M and Table
303 1). As expected given the fact that residues I, L, V, F and A, in decreasing order, display the

304 highest α-helix propensities in a non polar environment (36), computer predictions obtained
305 using the SSPro 2.01 software (SYMPRED server) and Membrane Protein Explorer (MPEx)
306 software version 3.0, respectively show that the α-helix conformation and the TM length of
307 p7B TMD are not disturbed by mutations (Table S2). A feasible conclusion that could be
308 drawn from these results is that an appropriate p7B TMD hydrophobicity value is required to
309 MNSV cell-to-cell movement.

310 *Mutation affecting p7B TMD secondary structure.* To test whether the p7B TMD secondary
311 structure was relevant in MNSV cell-to-cell movement, the $S_{23}P$ mutant was constructed.
312 Statistical studies have revealed that α-helical membrane-buried regions of non channel
313 proteins are largely devoid of intramembrane proline residues (13). The cyclic structure of this
314 amino acid strongly restricts the conformational space resulting in a redirection of the peptide
315 chain that can distort α-helix structures (13). According to this observation, the $S_{23}P$ mutation
316 abolished MNSV cell-to-cell movement (Fig. 2N and Table 1) whereas only a slight reduction
317 of local spread was observed when the same serine was changed to alanine (Fig. 2O and
318 Table 1). Thus, structural requirements are also critical for efficient MNSV cell-to-cell
319 movement.

320 *Mutations affecting the net charge distribution on either side of the p7B TMD.* The
321 membrane orientation of transmembrane proteins is primarily determined by the net charge
322 balance in the 13 to 25 residues flanking both sides of the TMD, whereby the more positive
323 end is predominantly positioned to the cytoplasmic side of the membrane. This phenomenon
324 is known as the “positive-inside rule” (34). Since p7B shows an identical net charge balance (-
325 1) on either side of the TMD, we decided to obtain the D_7R and $D_{44}R$ mutants, which resulted
326 in a negative-to-positive inversion of the net charge balance (-1 to +1) in the N_t and C_t

327 regions, respectively, to study the contribution of the positive-inside rule in MNSV cell-to-cell
328 movement. Despite the D_7R and $D_{44}R$ mutations possibly favoring wild-type and opposite p7B
329 membrane orientation, respectively, cell-to-cell movement was drastically reduced in both
330 cases (10-15%) (Fig. 2P and 2Q, respectively and Table 1).

331 *Mutations affecting p7B aromatic residues.* To study the implication of residues Y13
332 (putative "aromatic belt") and Y28 (putative snorkeling effector) in MNSV cell-to-cell
333 movement, we constructed the $Y_{13}A$ and the $Y_{28}A$ mutants. Unexpectedly, infected
334 fluorescent area of both mutants was greater than that obtained with wild-type RNA (Fig. 2R
335 and 2S, respectively and Table 1) whereas half-reduction of the local movement relative to
336 the wild-type was observed in the $Y_{39}A$ mutant. The location of the residue Y39 in a
337 conserved β-sheet conformation (42), which might be involved in alternative functions that are
338 also relevant in cell-to-cell movement, could explain the discrepancies observed (Fig. 2T and
339 Table 1). In this sense, the $Q_{35}AG_{36}AN_{37}A$ mutation located downstream of the TMD but not
340 affecting the conserved region produced only a 20% reduction in local movement relative to
341 the wild-type (Fig. 2U and Table 1).

342 **Distortion of the TMD secondary structure is the unique topological determinant**
343 **affecting p7B membrane association.**

344 In order to study whether the different topological determinants analyzed above affect the
345 p7B membrane association, four representative mutants were analyzed. The selected
346 mutants included: i) either the $L_{20}AF_{21}AI_{22}A$ or $I_{22}LS_{23}LF_{24}LV_{25}L$ mutation, which brought
347 about the greatest reduction or increase of TMD hydrophobicity, respectively; ii) the $D_{44}R$
348 mutation, which generates a positive net charge balance in the p7B C-terminal domain; and
349 finally iii) the $S_{23}P$ mutation, which most likely distorts the membrane-spanning α-helix. All

four mutations were individually introduced into the GFP-p7B binary construct and transiently expressed in *N. benthamiana* leaves. Membrane association status of mutant MPs was characterized by subcellular fractionation followed by different treatments as described before. Neither the $L_{20}AF_{21}AI_{22}A$, the $I_{22}LS_{23}LF_{24}LV_{25}L$ or the $D_{44}R$ mutations had an effect on membrane association given that the segregation between S and P fractions of mutant MPs was like wild-type p7B (Fig. 3). With the $S_{23}P$ mutant, the subcellular fractionation analysis revealed that a significant fraction of the protein (more than 50% of the signal) was recovered in the soluble fraction with no solubilization treatment (Fig. 3). Moreover, the $S_{23}P$ mutant fraction that remained associated with the membrane behaved like peripheral membrane proteins because it was partially and fully extracted with alkaline and 4M urea solutions, respectively (Fig. 3).

Next, we introduced the above mutations into the binary constructs expressing either N_t[YFP]-p7B or p7B-N_t[YFP] to study membrane orientation. It has been previously demonstrated that the N-terminus of a membrane protein is inserted first into the translocon (21). Thus, very hydrophobic TMDs leave no time for N-terminal re-orientation resulting in N_{lum}-C_{cyt} orientation whereas less hydrophobic TMDs delay their translocon exit leaving open the possibility for re-orientation of the N-terminus (21). In this scenario, the $L_{20}AF_{21}AI_{22}A$ and $I_{22}LS_{23}LF_{24}LV_{25}L$ mutants favor wild-type and opposite orientation, respectively. However, both mutants adopted wild-type orientation since ER fluorescence was observed when the corresponding p7B-N_t[YFP] and N_t[YFP]-p7B mutants were co-expressed with ER-Ct[YFP] and Ct[YFP], respectively, (Fig. 4A and 4D for the $L_{20}AF_{21}AI_{22}A$ mutant, Fig. 4E and 4H for the $I_{22}LS_{23}LF_{24}LV_{25}L$ mutant, respectively). Fluorescence was not observed in the opposite combinations (Fig. 4B and 4C for the $L_{20}AF_{21}AI_{22}A$ mutant, Fig. 4F and 4G for the $I_{22}LS_{23}LF_{24}LV_{25}L$ mutant, respectively). On the other hand, either p7B($S_{23}P$)-N_t[YFP] or

374 N_t[YFP]-p7B(S_{23}P) together with Ct[YFP] resulted in both nuclear and cytoplasmic
375 fluorescence (Fig. 4J and 4L, respectively) most likely as a consequence of the presence of a
376 soluble fraction of the S_{23}P mutant supporting the results previously observed in the
377 microsomal partitioning assay (Fig. 3). No fluorescence was visible with the p7B(S_{23}P)-
378 N_t[YFP] and ER-Ct[YFP] combination indicating that the C-terminal region of p7B(S_{23}P)-
379 N_t[YFP] is not translocated into the ER lumen (Fig. 4I).

380 The contribution of the positive-inside rule in p7B membrane orientation was assessed in
381 both the D_{44}R mutant and the +3K insertion mutant that contains three extra lysine residues
382 after the S32 position. Despite both mutant proteins should adopt a wild-type opposite
383 orientation according to the positive-inside rule, no topology inversion was observed (Fig. 4M
384 to 4P for the D_{44}R mutant and Fig. 4Q to 4T for the +3K mutant). These results contrast with
385 those previously reported in a prokaryotic system where topology inversion of a MNSV p7B-
386 GFP recombinant protein harboring the +3K insertion was achieved (40). This discrepancy
387 may be due to several factors: i) differences in the composition of the anionic phospholipids
388 between the *E. coli* inner membrane and the ER membrane of plant cells; ii) the absence of
389 electrochemical potential in plant ER membranes; and iii) the possibility that different solutions
390 to membrane insertion would operate in different organisms.

391 According to that, only the disruption of the TMD secondary structure producing an
392 alteration of the p7B membrane topology might explain the previously observed cell-to-cell
393 movement inhibition. However, since the topology of p7B was not substantially affected in the
394 remaining mutants, no direct correlation between non-competent cell-to-cell movement
395 phenotype and appropriate p7B insertion in the ER membrane can be drawn. These results
396 suggest that other factors influencing the functionality of p7B in viral movement were affected
397 in these mutants.

Trafficking of p7B to the cell periphery is affected at different stages in non-competent movement mutants.

Several studies have identified aromatic, charged and hydrophobic residues in addition to TMD hydrophobicity as structural determinants controlling the intracellular trafficking of proteins (4, 10). Thus, those mutations which were initially engineered to modify p7B topology may have also affected the ER-GA-Pd pathway followed by p7B to reach the Pd (20). To test this possibility, we introduced both competent and deficient movement mutations into the GFP-p7B recombinant protein. Agrobacterium-mediated transient expression was used to examine the subcellular localization of GFP-p7B mutants in *N. benthamiana* leaves. Until 36 h post agroinfiltration, expression of all mutant proteins resulted in a reticular staining pattern characteristic of ER localization (Fig. 5A and Table 1). Strong ER labeling was observed except for GFP-p7B($S_{23}P$), which faintly labeled this cellular compartment (scan of this mutant used a higher laser intensity than the rest).

At 48 h post agroinfiltration, ER labeling was scarcely observed except for GFP-p7B($I_{22}LS_{23}LF_{24}LV_{25}L$). In this case, the ER staining underwent morphological changes leading to the conversion of the tubular ER pattern into small cytoplasmic bodies that collapsed into large aggregates (Fig. 5B and 6G). Similar behavior was previously reported for TMV MP (45). When transiently expressed together in *N. benthamiana* leaves, TMV MP-mRFP and GFP-p7B($I_{22}LS_{23}LF_{24}LV_{25}L$) colocalized in the same ER aggregates (Fig. 5C), indicating that GFP-p7B($I_{22}LS_{23}LF_{24}LV_{25}L$) induces rearrangements of the plant ER membranes in contrast to GFP-p7B(wt). One possibility is that the $I_{22}LS_{23}LF_{24}LV_{25}L$ mutation retained the protein in the ER membrane, and that ER aggregates were an experimental artifact caused by its overexpression. In marked contrast, the remaining mutants were mostly localized in motile cytoplasmic vesicles (Fig. 6). These structures were visualized in

422 colocalization with the GA marker STtmdChFP but only when mutants were competent for
423 virus movement (Fig. 6A-B, 6D-F, 6I, 6J-K and Table 1). One exception was the $S_{23}P$ mutant,
424 which associated with the Golgi marker but the corresponding viral RNA did not move (Fig.
425 6H and Table 1).

426 Localization of MP to GA appears to be important for virus movement but it is not sufficient
427 for this activity. To further analyze whether the p7B post-Golgi transport to Pds was affected,
428 we transiently co-expressed GFP-p7B (Fig. 7A) and the different mutants (Fig 7B-J) with the
429 PNRSV MP, a Pd marker (2). GFP-p7B holding competent movement mutations (Fig. 7C-D,
430 7E, 7H-I and Table 1) generated fluorescent peripheral punctuate structures which
431 colocalized with the Pd marker. By contrast, GFP-p7B holding non-competent movement
432 mutations including GFP-p7B($S_{23}P$) were not localized to Pds (Fig. 7B, 7F-G, 7J and Table 1).
433 Overall, these data indicate that the mutations inhibiting virus cell-to-cell movement affect the
434 intracellular pathway of p7B to the cell periphery at different stages including ER exit, GA
435 targeting and post-Golgi transport.

436 **DISCUSSION**

437 The final topology of membrane proteins is determined by a set of intricate interactions
438 between the structural determinants of the protein, which are recognized by the translocon
439 complex, and the particular properties of the destination membrane. These properties include
440 lipid composition, cholesterol concentration, membrane thickness and electrochemical
441 potential (6, 14). Host-specific chaperones such as TRAM may also be required for
442 membrane insertion of viral MPs (50). The high variability of these properties among different
443 organisms emphasizes the importance of studying membrane protein structure/function
444 relationships in the native lipid environment context. In this work, live-cell fluorescence
445 imaging was performed to investigate the topology of MNSV p7B, a plant virus MP, in the ER

membrane of plant cells. MNSV p7B has been previously shown to integrate co-translationally into both canine pancreas microsomes and the *E. coli* inner membrane with an N_{cyt}-C_{lum} orientation (40, 42). We also demonstrated that GFP-p7B fusion was able to integrate into the plant ER membrane. Nevertheless, information about the contribution of the hydrophobic region to the process and about the orientation of the viral MP in the membrane is lacking (20).

The results presented herein reveal that the p7B TMD can promote efficient ER targeting and strong association of GFP with ER membranes, thus acting as an ER-targeting domain in plant cells. Although the plant GA has been reported to be the possible default destination for single-pass membrane proteins containing TMDs of about 19-20 amino acid in length (7), the p7B TMD by itself was unable to promote GFP transport from the ER to GA, resulting in ER retainment. Thus, MNSV p7B export from the ER appears to be controlled by specific export motifs located in the cytoplasmic and/or luminal domains. In the absence of these dominant motifs, ER retention may result from a better match between the lipid composition of the ER membrane and p7B TMD length/hydrophobicity. The p7B TMD clearly differs from the TMD of the plasmodesmata-located protein PLPd1a since this latter domain contains all the information required for the intracellular transport of heterologous proteins to Pd via the secretory pathway (56). Characterization of putative p7B ER export signals will be the subject of further investigation since p7B ORF does not contain any of the classical ER export sequences identified in single-spanning membrane proteins (4). A similar situation has been recently reported for the rice secretory carrier membrane protein 1 (SCAMP 1) for which the ER export signal is apparently unique (10).

On the other hand, there are many p7B structural properties that could participate in establishing its final topology. Among them, the more prominent are the length, hydrophobicity

and α-helix configuration of the TMD as well as the net balance charge of the extra-membrane TMD proximal regions. For an efficient insertion into the lipid bilayer, protein transmembrane segments require a minimum hydrophobicity threshold which must be markedly high for ER-targeting sequences like the p7B TMD (38). Accordingly to this assumption, a two-fold reduction of p7B TMD hydrophobicity was sufficient to eliminate cell-to-cell movement. Similar results were also obtained for the $I_{22}LS_{23}LF_{24}LV_{25}L$ mutant, whose thermodynamic properties for membrane insertion proved more favourable than that of the wild-type sequence, strongly suggesting the need of an appropriate hydrophobicity value for the p7B function in cell-to-cell movement. Intriguingly, both the insertion and membrane orientation of the $L_{20}AF_{21}AI_{22}A$ and $I_{22}LS_{23}LF_{24}LV_{25}L$ mutants, with the most reduced and increased TMD hydropathy, respectively, were apparently not affected. Moreover, non-competent mutations which either lower or increase TMD hydrophobicity strongly correlate with either incorrect intracellular targeting to unidentified cytoplasmic vesicles or a drastic rearrangement of ER membranes, respectively, which impeded the ability of p7B to access the Pd. It is well-known that plant viruses need to exploit Pd to move from cell to cell in a process where virus-encoded movement proteins play a central role. Therefore, the ability of p7B to function in viral movement most likely depends on Pd localization which is defective in non competent cell-to-cell movement phenotypes. We can conclude that the p7B TMD controls the insertion of the MP into the ER membrane and can also modulated the next cellular destination of the MP in the presence of the ER export motifs located at the cytoplasmic and/or luminal domains.

There are three different TMD determinants controlling the subcellular localization of a membrane protein: the length of the TMD, the presence of specific sequence elements and the overall hydrophobic profile (7, 9, 56). We found that the length of the predicted p7B TMD

494 was unaffected by mutations and that the p7B TMD itself was unable to transport GFP out of
495 the ER. Therefore, other biophysical features of the TMD, such as the overall hydrophobicity
496 profile, modulate the proper targeting of the MP. Accordingly, changes in the hydropathy
497 profile of the TMD present in ER-resident cytocrome P450 2C1 also cause mislocation to
498 different subcellular compartments in COS1 cells (54). Moreover, the sarcolemmal
499 membrane-associated protein (SLMAP) possesses two alternatively spliced transmembrane
500 regions (tail anchor TA1 or TA2); TA2 is less hydrophobic than TA1 and determines the
501 subcellular localization of the SLMAP in the mitochondria, while SLMAP-TA1 is targeted to the
502 ER. However, the TA2-4L mutant has a transmembrane region that is only slightly less
503 hydrophobic than the wild type TA1 and it shares similar TA1 targeting properties (9). It is
504 tempting to speculate that large variations below or above wild-type p7B TMD hydrophobicity
505 affect the balance between TMD-membrane lipids interaction and signal-mediated export
506 resulting in different outcomes depending on TMD strength. For example, p7B ER-retention
507 dictated by the strong TMD hydrophobicity of the $I_{22}LS_{23}LF_{24}LV_{25}L$ mutant predominated over
508 the p7B ER-export signals located at the extramembrane domains. Addition of a diacidic
509 export motif suppresses the ER retention of the *Yellow fever protein* (YFV) E envelope protein
510 that is mediated by a TMD, but the same tagging did not override the ER retention signal of
511 the TMD from the YFV prM envelope protein (12).

512 Although many transmembrane α-helices contain bends and other distortions that have
513 important implications for protein function (47, 58), the proline-induced kink resulting from the
514 $S_{23}P$ mutation substantially affected the topology and intracellular transport of p7B as well as
515 viral cell-to-cell movement. The effect of the S23P mutation on MP membrane insertion was
516 most likely due to the central position of the proline within the TMD (25). The distorted helix
517 was likely too short to be well-accommodated into the hydrophobic core of ER membrane

518 generating a negative hydrophobic mismatch. In this situation, transmembrane helices can
519 adopt a surface orientation rather than a membrane-inserted state as occurred in $S_{23}P$ mutant
520 (46). Unexpectedly, this weak membrane association was sufficient to promote ER to GA
521 transport but not post-Golgi targeting to Pd. This indicates that membrane insertion is
522 essential for the p7B function in virus movement.

523 It is largely accepted that charged residues flanking the hydrophobic stretch strongly
524 modulate protein orientation relative to the membrane. A positive-inside rule seems to apply
525 universally to all the integral membrane proteins by which positively charged residues are
526 predominantly found in the flanking sequence that remains exposed to the cytosol. Our
527 results showed that p7B always adopts a N_{cyt}-C_{lum} orientation in planta although no biased
528 distribution of positively charged residues between cytoplasmic and ER luminal segments was
529 observed. Mutations that violate the positive-inside rule can prevent insertion of a TMD.
530 However, p7B was efficiently inserted into the ER membrane in the correct membrane
531 orientation when a negative to positive inversion of the Ct domain net charge was obtained in
532 both the $D_{44}R$ and the +3K mutants. A similar override of the positive-inside rule has been
533 described for the polytopic channel that constitutes the ductin protein and mitochondrial inner
534 membrane proteins (15, 17). Critical contribution of charged residues to intracellular transport
535 of p7B and MNSV cell-to-cell movement most likely relates to its involvement in interactions
536 with host and/or viral factors. Interestingly, point mutations affecting charged residues
537 introduced into ER luminal or cytosolic segments of BYV p6 resulted in a drastic reduction of
538 cell-to-cell movement (44). However, neither the topology nor the subcellular localization of
539 these BYV p6 mutants was studied.

540 Orientation of proteins in membranes can also be controlled by both TMD length and
541 hydrophobicity. Long and very hydrophobic TMDs favor translocation of the N-terminus

542 across ER membranes (N_{lum}-C_{cyt} orientation) whereas short and less hydrophobic segments
543 adopt an N_{cyt}-C_{lum} topology. However, a two-fold increase in TMD hydrophobicity of wild-type
544 p7B ($I_{22}LS_{23}LF_{24}LV_{25}L$ mutant) did not result in the opposite membrane orientation. BYV p6 is
545 structurally very similar to MNSV p7B but it shows an N_{lum}-C_{cyt} orientation in plant ER
546 membranes. BYV p6 exhibits a positive charge bias (+2) for the cytoplasmic Ct domain and
547 its TMD is longer (23 residues) and more hydrophobic ($\Delta G_{app(p6)}$ = -6.094 kcal mol^{-1}) than wild-
548 type p7B TMD. Therefore, a simultaneous and/or a higher modification of the putative
549 topological determinants might be necessary to invert the p7B membrane orientation,
550 suggesting a strong stability of the MP in the ER membrane. Similar results have also been
551 reported for *Carnation mottle virus* p9 MP using a heterologous system (51).

552 Finally, according to the observation that movement-competent p7B mutations do not affect
553 p7B subcellular localization, both the $Y_{13}A$ and the $Y_{28}A$ mutants were properly targeted to
554 ER, GA and Pd but unexpectedly, local spread of the corresponding mutant RNAs was
555 significantly higher than that of wild-type RNA. The Y13 residue is located at the amino end of
556 the TMD. After membrane insertion, it is most likely to be positioned at the membrane-
557 cytoplasm interface. Interfacial aromatic residues, commonly found among membrane
558 proteins, are important for the positioning and anchoring of the TMD in the lipid bilayer. In this
559 scenario, the precise positioning of p7B relative to the membrane does not appear essential
560 for its function but; nonetheless, the lack of anchoring restrictions can favor lateral mobility of
561 the p7B between different ER subdomains (for example, ER export sites or ERES) resulting in
562 an increased intracellular transport efficiency which, consequently, may facilitate MNSV local
563 infection progress. A similar effect can be produced when the snorkelling effect of Y28 was
564 removed.

In summary, the results presented herein demonstrate that the p7B Golgi-mediated traffic to Pd is essential for efficient MNSV cell-to-cell movement. Moreover, the multiple structural requirements of the MP appear to be involved in controlling Pd targeting. This probably reflects the multiple interactions that must occur between cellular factors and this small MP to guarantee functionality in the appropriate destination, the Pd. Similarly, multiple cytosolic and transmembrane determinants are also required for SCAMP 1 trafficking via an ER/GA/*trans*-Golgi network/plasma membrane pathway (10). Therefore, the reduced size and simple topology of p7B make this a useful system to gain a better understanding of not only the trafficking mechanism of single transmembrane proteins but of the interactions produced taking place between the viral protein and the cellular environment during the viral life cycle.

ACKNOWLEDGEMENTS

The work in our laboratory has been supported by grant BIO08-03528 from the Spanish granting agency DGICYT and by grant ACOMP 2011-074 from the Generalitat Valenciana. J. A. N. and A. G. are recipients of a postdoctoral contract and a PhD fellowship from the Spanish Ministerio de Ciencia e Innovación. We thank Dra. M.C. Herranz for critical reading of the manuscript and Dr V.V. Dolja (Oregon State University, Corvallis) for kindly providing the STtmdChFP and MP(TMV)-mRFP binary vectors. PNRSV MP and mGFP5 binary vectors were a generous gift of Dr. J. A. Sánchez (IBMCP, Valencia) and Dr. C. Torres (IBMCP, Valencia), respectively. We thank L. Corachán and L. Latorre for their technical assistance.

584 **REFERENCES**

585 1. Adams, M.J. and J.F. Antoniw. 2005. Membrane proteins from plant viruses *in* Viral
586 membrane proteins: structure, function, and drug design, Wolfgang B. Fischer ed. Kluwer
587 Academic/Plenum Publishers, New York. pp 3-20.
588 2. Aparicio, F., V. Pallás and J.A. Sánchez-Navarro. 2010. Implication of the C terminus of the
589 Prunus necrotic ringspot virus movement protein in cell-to-cell transport and in its
590 interaction with the coat protein. J. Gen. Virol. **91:**1865-1870.
591 3. Aparicio, F., J.A. Sánchez-Navarro and V. Pallás. 2006. *In vitro* and *in vivo* mapping of the
592 Prunus necrotic ringspot virus coat protein C-terminal dimerization domain by bimolecular
593 fluorescence complementation. J. Gen. Virol. **87:**1745-50.
594 4. Barlowe, C. 2003. Signals for COPII-dependent export from the ER: what's the ticket out?.
595 Trends Cell Biol. **13:**295-300.
596 5. Bechinger, B. 2001. Membrane insertion and orientation of polyalanine peptides: A 15N
597 solid-state NMR spectroscopy investigation. Biophys. J. **81:**2251-2256.
598 6. Brambillasca, S., ;M. Yabal, P. Soffientini, S. Stefanovic, M. Makarow, R.S. Hedge and N.
599 Borgesse. 2005. Transmembrane topogenesis of a tail-anchored protein is modulated by
600 membrane lipid composition. EMBO J. **24:**2533-2542.
601 7. Brandizzi, F., N. Frangne, S. Marc-Martin, C. Hawes, J.M. Neuhaus and N. Paris. 2002.
602 The destination for single-pass membrane proteins is influenced markedly by the length of
603 the hydrophobic domain. Plant Cell **14:**1077-1092.
604 8. Brill, L.M., R.S. Nunn, T.W. Kahn, M. Yeager and R.N. Beachy. 2000. Recombinant
605 Tobacco mosaic virus movement protein is an RNA-binding, alpha-helical membrane
606 protein. Proc. Natl. Acad. Sci. USA **97:**7112-7117.

9. Byers, J.T., R.M. Guzzo, M. Salih and B.S. Tuana. 2009. Hydrophobic profiles of the tail anchors in SLMAP dictate subcellular targeting. BMC Cell Biol. **10:**48.

10. Cai, Y., T. Jia, S.K. Lam, Y. Ding, C. Gao, M.W. San, P. Pimpl and L. Jiang. 2011. Multiple cytosolic and transmembrane determinants are required for the trafficking of SCAMP1 via an ER-Golgi-TGN-PM pathway. Plant J. no. doi: 10.1111/j.1365-313X.2010.04469.x.

11. Chamberlain, A.K., Y. Lee, S. Kim and J.U. Bowie. 2004. Snorkeling preferences foster an amino acid composition bias in transmembrane helices. J Mol Biol. **339:**471-479.

12. Ciczora, Y., N. Callens, K. Séron, Y. Rouillé and J. Dubuisson. 2010. Identification of a dominant endoplasmic reticulum-retention signal in yellow fever virus pre-membrane protein. J. Gen. Virol. **91:**404-414.

13. Deber, C.M. and A.G. Therien. 2002. Putting the β-breaks on membrane protein misfolding. Nat. Struct. Biol. **9:**318-319.

14. Dowhan, W. and M. Bogdanov. 2009. Lipid-dependent membrane protein topogenesis. Annu. Rev. Biochem. **78:**515-540.

15. Dunlop, J., P.C Jones and M.E. Finbow. 1995. Membrane insertion and assembly of ductin: a polytopic channel with dual orientation. EMBO Journal **14:**3609-3616.

16. Fujiki, M., S. Kawakami, R.W. Kim and R.N. Beachy. 2006. Domains of tobacco mosaic virus movement protein essential for its membrane association. J. Gen. Virol. **9:**2699-2707.

17. Gavel, Y. and G. von Heijne. 1992. The distribution of charged amino acids in mitochondrial inner-membrane proteins suggests different modes of membrane integration for nuclearly and mitochondrially encoded proteins. Eur. J. Biochem. **205:**1207-1215.

18. Genovés, A., J.A. Navarro and V. Pallás. 2006. Functional analysis of the five Melon necrotic spot virus genome-encoded proteins. J. Gen. Virol. **87:**2371-2380.

631 19. Genovés, A., J.A. Navarro and V. Pallás. 2009. A self-interacting carmovirus
632 movement protein plays a role in binding of viral RNA during the cell-to-cell movement and
633 shows an actin cytoskeleton dependent location in cell periphery. Virology **395:**133-142.
634 20. Genovés, A., J.A. Navarro and V. Pallás. 2010. The intra- and intercellular movement
635 of Melon necrotic spot virus (MNSV) depends on an active secretory pathway. Mol. Plant
636 Microbe Interact. **23:**263-272.
637 21. Goder, V. and M. Spiess. 2003. Molecular mechanism of signal sequence orientation in
638 the endoplasmic reticulum. EMBO J. **22:**3645-3653.
639 22. Granseth, E., G. von Heijne and A. Elofsson. 2005. A study of the membrane-water
640 interface region of membrane proteins. J. Mol. Biol. **346:**377-385.
641 23. Guenoune-Gelbart, D., M. Elbaum, G. Sagi, A. Levy and B.L. Epel. 2008. *Tobacco*
642 *mosaic virus* (TMV) replicase and movement protein function synergistically in facilitating
643 TMV spread by lateral diffusion in the plasmodesmal desmotubule of *Nicotiana*
644 *benthamiana*. Mol. Plant Microbe Interact. **21:**335-345.
645 24. Harries, P.A., J.W. Park, N. Sasaki, K.D. Ballard, A.J. Maule and R.S. Nelson. 2009.
646 Differing requirements for actin and myosin by plant viruses for sustained intercellular
647 movement. Proc. Natl. Acad. Sci. USA. **106:**17594-17599.
648 25. Hessa, T., H. Kim, K. Bihlmaier, C. Lundin, J. Boekel, H. Andersson, I. Nilsson, S.H.
649 White and G. von Heijne 2005. Recognition of transmembrane helices by the endoplasmic
650 reticulum translocon. Nature **433:**377-381.
651 26. Hessa, T., S.H. White, and G. von Heijne. 2005. Membrane insertion of a potassium
652 channel voltage sensor. Science **307:**1427.

27. Hessa, T., N.M. Meindl-Beinker, A. Bernsel, H. Kim, Y. Sato, M. Lerch-Bader, I. Nilsson, S.H. White and G. von Heijne. 2007. Molecular code for transmembrane-helix recognition by the Sec61 translocon. Nature **450:**1026-1030.

28. Huang, M., L. Jongejan, H. Zheng, L. Zhang and J.F. Bol. 2001. Intracellular localization and movement phenotypes of *Alfalfa mosaic virus* movement protein mutants. Mol. Plant Microbe Interact. **14:**1063-1074.

29. Huang, M. and L. Zhang. 1999. Association of the movement protein of *Alfalfa mosaic virus* with the endoplasmic reticulum and its trafficking in epidermal cells of onion bulb scales. Mol. Plant-Microbe Interact. **12:**680-690.

30. Higy, M., T. Junne and M. Spiess. 2004. Topogenesis of membrane proteins at the endoplasmic reticulum. Biochemistry **43:**12716-12722.

31. Kawakami, S., Y. Watanabe and R.N. Beachy. 2004. Tobacco mosaic virus infection spreads cell to cell as intact replication complexes. Proc. Natl. Acad. Sci. USA **101:**6291-6296.

32. Knoester, M., L.C. van Loon, J. van den Heuvel, J. Hennig, J.F. Bol and H.J.M. Linthorst. 1998. Ethylene-insensitive tobacco lacks non-host resistance against soil-borne fungi. Proc. Natl. Acad. Sci. USA **95:**1933-1937.

33. Laliberté, J.F. and H. Sanfaçon. 2010. Cellular remodeling during plant virus infection. Annu. Rev. Phytopathol. **48:**69-91.

34. Lerch-Bader, M., C. Lundin, H. Kim, I. Nilsson and G. von Heijne. 2008. Contribution of positively charged flanking residues to the insertion of transmembrane helices into the endoplasmic reticulum. Proc. Natl. Acad. Sci. U S A **105:**4127-4132.

675 35. Liang, J., L. Adamian and R. Jr. Jackups. 2005. The membrane–water interface region
676 of membrane proteins: structural bias and the anti-snorkeling effect. Trends Biochem. Sci.
677 **30:**355-357.
678 36. Liu, L.P. and C.M. Deber. 1999. Combining hydrophobicity and helicity: a novel
679 approach to membrane protein structure prediction. Bioorg. med. Chem. **7**:1-7.
680 37. Lucas, W.J. 2006. Plant viral movement proteins: agents for cell-to-cell trafficking of
681 viral genomes. Virology **344:**169-184.
682 38. Lundin, C., H. Kim, I. Nilsson, S. White and G. von Heijne. 2008. The molecular code
683 for protein insertion in the ER membrane is similar for N_{in}–C_{out} and N_{out}–C_{in} transmembrane
684 helices. Proc. Natl. Acad. Sci. USA **105:**15702-15707.
685 39. Mandahar, C.L. 2006. Multiplication of RNA plant virus. Springer-Verlag ed. Dordrecht,
686 The Netherlands.
687 40. Martínez-Gil, L., A. Saurí, M. Vilar, V. Pallás and I. Mingarro. 2007. Membrane insertion
688 of the p7B movement protein of *Melon necrotic spot virus* (MNSV). Virology **367:**348-357.
689 41. Martínez-Gil, L., J.A. Sánchez-Navarro, A. Cruz, V. Pallás, J. Pérez-Gil and I. Mingarro.
690 2009. Plant virus cell-to-cell movement is not dependent on the transmembrane disposition
691 of its movement protein. J. Virol. **83:**5535-5543.
692 42. Navarro, J.A., A. Genovés, J. Climent, A. Saurí, L. Martínez-Gil, I. Mingarro, and V.
693 Pallás. 2006. RNA-binding properties and membrane insertion of Melon necrotic spot virus
694 (MNSV) double gene block movement proteins. Virology **356:**57-67.
695 43. Nilsson, J., B. Persson and G. von Heijne. 2005. Comparative analysis of amino acid
696 distributions in integral membrane proteins from 107 genomes. Proteins **60:**606-616.

44. Peremyslov, V.V., Y.W. Pan and V.V. Dolja. 2004. Movement protein of a closterovirus is a type III integral transmembrane protein localized to the endoplasmic reticulum. J. Virol. **78:**3704-3709.

45. Reichel, C. and R.N. Beachy. 1998. Tobacco mosaic virus infection induces severe morphological changes of the endoplasmic reticulum. Proc. Natl. Acad. Sci. USA **19:**11169-11174.

46. Ren, J., S. Lew, Z. Wang and E. London. 1997. Transmembrane orientation of hydrophobic α-helices is regulated both by the relationships of helix length to bilayer thickness and by cholesterol concentration. Biochemestry **36:**10213-10220.

47. Riek, R.P., I. Rigoutsos, J. Novotny and R.M. Graham. 2001. Non-alpha-helical elements modulate modulate polytopic membrane protein architecture. J. Mol. Biol. **306:**349-362.

48. Sambade, A. and M. Heinlein. 2009. Approaching the cellular mechanism that supports the intercellular spread of *Tobacco mosaic virus*. Plant Signal Behav. **4:**35-38.

49. Sagi, G., A. Katz, D. Guenoune-Gelbart and B.L. Epel. 2005. Class 1 reversibly glycosylated polypeptides are plasmodesmal-associated proteins delivered to plasmodesmata via the golgi apparatus. Plant Cell **17:**1788-800.

50. Saurí, A., P.J. McCormick, A.E. Johnson and I. Mingarro. 2007. Sec61alpha and TRAM are sequentially adjacent to a nascent viral membrane protein during its ER integration. J. Mol. Biol. **366:**366-374.

51. Saurí, A., S. Tamborero, L. Martínez-Gil, A.E. Johnson and I. Mingarro. 2009. Viral membrane topology is dictated by multiple determinants in its sequence. J. Mol. Biol. **387:**113-128.

720 52. Scholthof, H.B. 2005. Plant virus transport: motions of functional equivalence. Trends
721 Plant Sci. **10:**376-382.
722 53. Schwartz, M., J. Chen, W.-M. Lee, M. Janda and P. Ahlquist. 2004. Alternate, virus-
723 induced membrane rearrangements support positive-strand RNA virus genome replication.
724 Proc. Natl. Acad. Sci. USA. **101:**11263-11268.
725 54. Szczesna-Skorupa, E. and B. Kemper. 2000. Endoplasmic reticulum retention
726 determinants in the transmembrane and linker domains of cytochrome P450 2C1. J. Biol.
727 Chem. **275:**19409-19415.
728 55. Taliansky, M., L. Torrance and N.O. Kalinina. 2008. Role of plant virus movement
729 proteins. Methods Mol. Biol. **451:**33-54.
730 56. Thomas, C., E.M. Bayer, C. Ritzenthaler, L. Fernandez-Calvino, and A.J. Maule. 2008.
731 Specific targeting of a plasmodesmal protein affecting cell-to-cell communication. PLOS
732 Biology **6:**1-11.
733 57. Verchot-Lubicz, J., L. Torrance, A.G. Solovyev, S.Y. Morozov, A.O. Jackson and D.
734 Gilmer. 2010. Varied movement strategies employed by triple gene block-encoding viruses.
735 Mol. Plant Microbe Interact. **23:**1231-1247.
736 58. von Heijne, G. 1991. Proline kinks in transmembrane α-helices. J. Mol. Biol. **218:**499-
737 503.
738 59. von Heijne, G. 2006. Membrane-protein topology. Nat. Rev. Mol. Cell Biol. **7:**909-918.
739 60. von Heijne, G. 2007. Formation of transmembrane helices *in vivo* -is hydrophobicity all
740 that matters? J. Gen. Physiol. **129:**353-356.
741 61. White, S.H. and G. von Heijne. 2005. Transmembrane helices before, during and after
742 insertion. Curr. Opin. Struct. Biol. **15:**378-386.

62. Zamyatnin, A.A.Jr., A.G. Solovyev, P.V. Bozhkov, J.P. Valkonen, S.Y. Morozov and E.I. Savenkov. 2006. Assessment of the integral membrane protein topology in living cells. Plant J. **46:**145-154.

746

Table 1. List of p7B mutations set into structural feature groups and summary of results obtained in cell-to-cell movement assays and subcellular localization experiments.

Mutation	Structural feature	ΔG_{app} (kcal mol^{-1})	Movement %	Subcellular localization		
				ER	GA	Pd
wt		-1.869	100	+	+	+
$L_{17}AL_{18}AI_{19}A$	TMD[1] hydrophobicity	-0.493	0	+	-	-
$L_{20}AF_{21}AI_{22}A$		-0.408	0	+	-	-
$F_{24}AV_{25}AF_{26}A$		-0.878	0	n.a.[2]	n.a.	n.a.
$F_{27}AI_{29}AL_{32}A$		-0.916	0	n.a.	n.a.	n.a.
$F_{27}AY_{28}AI_{29}A$		-1.164	0	n.a.	n.a.	n.a.
$F_{27}AI_{29}A$		-1.191	0	+	-	-
$I_{22}AS_{23}AF_{24}AV_{25}A$		-1.465	81	+	+	+
$L_{18}A$		-1.472	72	+	+	+
$F_{21}A$		-1.563	86	+	+	+
$V_{25}A$		-1.682	66	+	+	+
$F_{24}LV_{25}LF_{26}L$		-2.383	87	+	+	+
$I_{22}LS_{23}LF_{24}LV_{25}L$		-3.630	9.7	+	-	-
$Q_{35}AG_{36}AN_{37}A$	triple mutant control	-1.869	80	+	+	+
D_7R	net balance charge	-1.869	12	+	-	-
$D_{44}R$		-1.869	16	+	-	-
$Y_{13}A$	aromatic residues	-1.725	154	+	+	+
$Y_{28}A$		-1.842	123	+	+	+
$Y_{39}A$		-1.869	54	+	+	+
$S_{23}P$	α-helix	-1.384	0	+	+	-
$S_{23}A$	control Ser23	-2.598	93	+	+	+

[1] *Transmembrane domain*, [2] *not assayed*

747

FIG. 1. Characterization of MNSV p7B topology in plant ER membranes. (A) Open reading frame (ORF) of MNSV p7B and a schematic representation of the expression cassette in which amino acid sequence corresponding to the p7B computer-predicted transmembrane domain (TMD) was cloned (pMGFP-tmd(p7B)). 35S, *Cauliflower mosaic virus* 35S promoter. PoPit, potato proteinase inhibitor II terminator. (B and C) Transient expression of GFP-tmd(p7B) (B) and the luminal ER marker, mGFP5-KDEL (C). A reticular staining pattern, which is indicative of ER localization, was observed in both proteins. (D and E) Colocalization of GFP-p7B (green channel, D) and the Golgi-specific marker, STtmdChFP (red channel not shown). Merged image of both green and red channels is shown in panel E. Confocal microscopy images are representative of those taken in three independent experiments at 48 h post agroinfiltration. (F) Microsomal partitioning of tissue extracts from *N. benthamiana* leaves either expressing GFP-p6(BYV), GFP-p7B, or GFP-tmd(p7B). After high-speed centrifugation, untreated pellet containing microsomes (P) and supernatant (S) fractions were obtained. Alternatively, the P fraction was subjected to different treatments and separated again into S and P fractions by ultracentrifugation. Equivalent amounts of both untreated and treated S and P fractions were subjected to SDS-PAGE and analyzed by immunoblotting with anti-GFP antibodies. (G to N) Assessment of MNSV p7B orientation in plant ER membranes using a bimolecular fluorescence complementation (BiFC) based assay. Images correspond to single confocal microscopy scans obtained at 36 h post agroinfiltration in *N. benthamiana* leaves of the protein combinations indicated in the upper right side of each panel. Silencing supressor HC-Pro was included in all co-expression assays. Scale bars correspond to 20 μm except where indicated. Images from panels G to N are pseudocolored in green.

FIG. 2. Contribution of p7B topological determinants in viral cell-to-cell movement. (A) Schematic representation of the recombinant infectious clone pMNSV(Al)-Δcp-GFP in which

MNSV CP was replaced by the GFP gene. Secondary structure illustration and open reading frame (ORF) of p7B are shown bellow. Viral and fluorescent protein names are indicated. The conserved α-helix/transmembrane domain and β-sheet structures are represented by a box and jagged lines, respectively. MNSV p7B residues affected by mutations are shown in red. Subheading numbers indicate protein residue position. (B to U) Confocal microscopy scans taken at 2-3 days post inoculation of both wild-type and mutant RNAs in melon plant cotyledons. Images are representative of infection foci observed in three independent experiments. Viral RNAs were generated by *in vitro* transcription of the corresponding pMNSV(AI)-Δcp-GFP variant. Mutations are indicated in the upper right side of each panel. Scale bars correspond to 200 μm except where indicated.

FIG. 3. Membrane association analysis of GFP-p7B mutants. Extracts from *N. benthamiana* leaves either expressing GFP-p7B, GFP-p7B($L_{20}AF_{21}AI_{22}A$), GFP-p7B($I_{22}LS_{23}LF_{24}LV_{25}L$), GFP-p7B($D_{44}R$) or GFP-p7B($S_{23}P$) were separated into pellet (P) and supernatant (S) fractions by high-speed centrifugation (untreated fractions). The P fractions were divided in several aliquots and treated either with 0.1M Na_2CO_3 (pH 11), 4 M urea or 1% Triton X-100 plus 0.5M NaCl. Samples were again separated into S and P fractions by ultracentrifugation. Equivalent amounts of untreated and treated S and P fractions were subjected to SDS-PAGE and analyzed by immunoblotting with anti-GFP antibodies.

FIG. 4. Membrane orientation analysis in plant ER membranes of the p7B($L_{20}AF_{21}AI_{22}A$) (A to D), p7B($I_{22}LS_{23}LF_{24}LV_{25}L$) (E to H), p7B($S_{23}P$) (I to L), p7B($D_{44}R$) (M-P) and p7B(+3K) (Q to T) mutants using a bimolecular fluorescence complementation (BiFC) based assay. Images correspond to single confocal microscopy scans obtained 36 h post agroinfiltration in *N. benthamiana* leaves of the constructs combinations indicated as follows: first and second

panels rows correspond to coexpression of p7B-Nt[YFP] mutants with either ER-Ct[YFP] or Ct[YFP], respectively; third and fourth panels rows correspond to coexpression of Nt[YFP]-p7B mutants with either ER-Ct[YFP] or Ct[YFP], respectively. Mutations are indicated under each panel column. Silencing supressor HC-Pro was included in all coexpression assays. Scale bars correspond to 20 μm. Images are pseudocolored in green.

FIG. 5. (A) Subcellular localization of wild type and mutants of GFP-p7B in the endoplasmic reticulum (ER). Confocal microscopy scans were taken at 36 h post agroinfiltration in *N. benthamiana* leaves. Scale bar corresponds to 15 μm. A complete review of the results can be found in the Table 1. Mutations are indicated in the upper left side of each panel. (B) Confocal images of *Nicotiana benthamiana* epidermical cells expressing GFP-p7B($I_{22}LS_{23}LF_{24}LV_{25}L$) taken at 48 h post agroinfiltration. Images show how ER staining obtained after GFP-p7B($I_{22}LS_{23}LF_{24}LV_{25}L$) expression underwent morphological changes leading to the conversion of the tubular ER pattern (region enclosed in the square 1 on the left panel) into small cytoplasmic bodies (region enclosed in the square 2 on the left panel) that collapsed into large aggregates (panel on the right). (C) Colocalization of TMV MP-mRFP (panel on the left) and GFP-p7B($I_{22}LS_{23}LF_{24}LV_{25}L$) (image not shown) into ER aggregates at 48 h post agroinfiltration in *N. benthamiana* leaves. The merged image of green and red channels is shown (right panel).

FIG. 6. Coexpression of wild-type and mutants of GFP-p7B ("GFP-p7B" panel columns) with the Golgi apparatus (GA) marker STtmdChFP ("STtmdChFP" panel columns). Merged images of green and red channels are shown in the "overlay" columns. Confocal images correspond to coexpression of the GA marker with either the wild type GFP-p7B (A), the $Q_{35}AG_{36}AN_{37}A$ mutant (B), the $L_{20}AF_{21}AI_{22}A$, $L_{18}A$, $I_{22}AS_{23}AF_{24}AV_{25}A$, $F_{24}LV_{25}LF_{26}L$ and

$I_{22}LS_{23}LF_{24}LV_{25}L$ mutants affecting p7B transmembrane domain hydrophobicity (TMD) (C to G, respectively), the $S_{23}P$ mutant affecting the α-helix structure of the p7B TMD (H), the $S_{23}A$ mutant used as control of the $S_{23}P$ mutant (I), the $Y_{13}A$ mutant lacking the Y13 putative aromatic belt (J), the $Y_{39}A$ mutant affecting the conserved β-sheet structure at the p7B C-terminal domain (K) or the $D_{44}R$ mutant displaying a C-terminal bias of positively charged amino acids (L). Mutations are indicated in the overlay panels. Confocal microscopy scans were taken at 48 h after agroinfiltration. Scale bars correspond to 8 μm. A complete review of the results can be found in the Table 1.

FIG. 7. Coexpression of wild type and mutants of GFP-p7B ("GFP-p7B" panel columns) with the plasmodesmata marker, PNRSV MP-ChFP ("PNRSV MP-ChFP" panel columns). Merged images of green and red channels are shown in the "overlay" columns. Confocal images correspond to coexpression of the Pd marker with either the wild-type GFP-p7B (A), the $L_{20}AF_{21}AI_{22}A$, $L_{18}A$, $I_{22}AS_{23}AF_{24}AV_{25}A$, $F_{24}LV_{25}LF_{26}L$ or $I_{22}LS_{23}LF_{24}LV_{25}L$ mutants affecting p7B transmembrane domain (TMD) hydrophobicity (B to F, respectively), the $S_{23}P$ mutant affecting the α-helix structure of the p7B TMD (G), the $S_{23}A$ mutant used as control of the $S_{23}P$ mutant (H), the $Y_{13}A$ mutant lacking the Y13 putative aromatic belt (I) or the $D_{44}R$ mutant displaying a C-terminal bias of positively charged amino acids (J). Mutations are indicated in the overlay panels. Scale bars correspond to 8 μm. Confocal microscopy scans were taken at 48 h after agro-infiltration. A complete review of the results can be found in the Table 1.

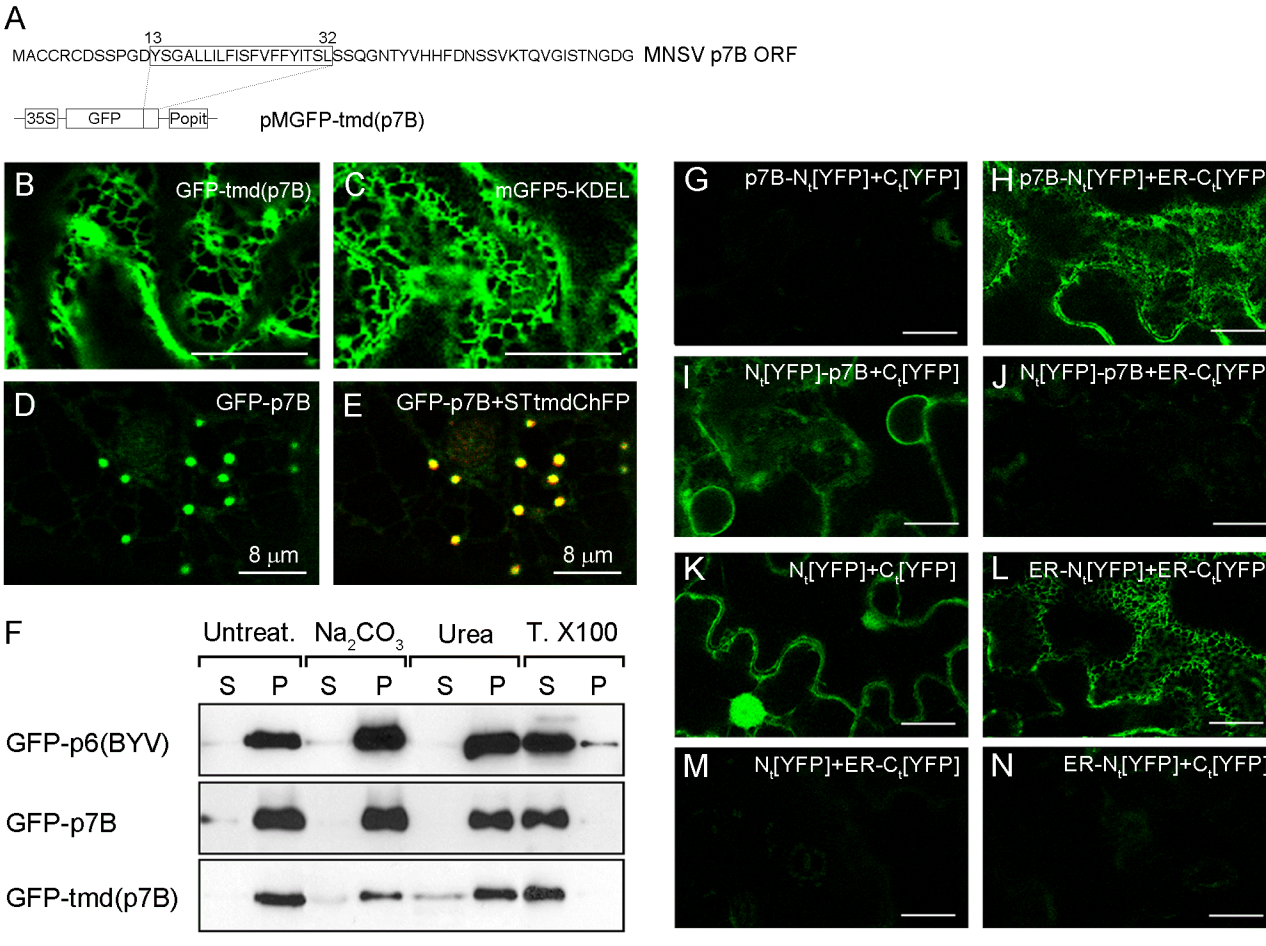
A
13
32
MACCRCDSSPGDYSGALLILFISFVFFYITSLSSQGNTYVHHFDNSSVKTQVGISTNGDG MNSV p7B ORF
35S
GFP
Popit
pMGFP-tmd(p7B)
B GFP-tmd(p7B)
C mGFP5-KDEL
D GFP-p7B
8 μm
E GFP-p7B+STtmdChFP
8 μm
F
Untreat.
Na2CO3
Urea
T. X100
S P S P S P S P
GFP-p6(BYV)
GFP-p7B
GFP-tmd(p7B)
G p7B-Nt[YFP]+Ct[YFP]
H p7B-Nt[YFP]+ER-Ct[YFP]
I Nt[YFP]-p7B+Ct[YFP]
J Nt[YFP]-p7B+ER-Ct[YFP]
K Nt[YFP]+Ct[YFP]
L ER-Nt[YFP]+ER-Ct[YFP]
M Nt[YFP]+ER-Ct[YFP]
N ER-Nt[YFP]+Ct[YFP]

FIG. 1

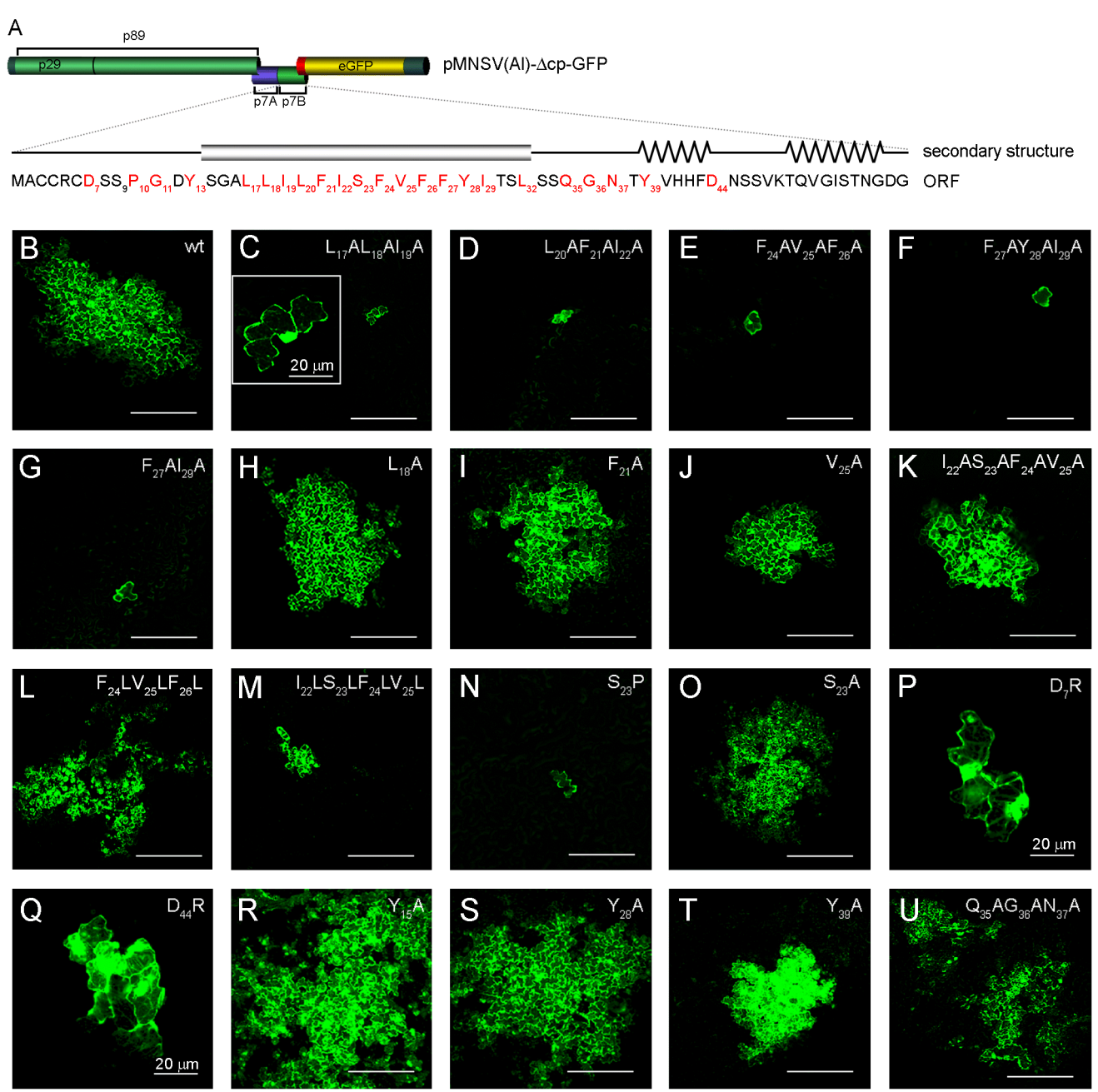
A
p89
p29
eGFP
pMNSV(AI)-Δcp-GFP
p7A p7B
secondary structure
MACCRCD7SS9P10G11DY13SGAL17L18I19L20F21I22S23F24V25F26F27Y28I29TSL32SSQ35G36N37TY39VHHFD44NSSVKTQVGISTNGDG ORF
B wt
C L17AL18AI19A
20 μm
D L20AF21AI22A
E F24AV25AF26A
F F27AY28AI29A
G F27AI29A
H L18A
I F21A
J V25A
K I22AS23AF24AV25A
L F24LV25LF26L
M I22LS23LF24LV25L
N S23P
O S23A
P D7R
20 μm
Q D44R
20 μm
R Y15A
S Y28A
T Y39A
U Q35AG36AN37A

FIG. 2

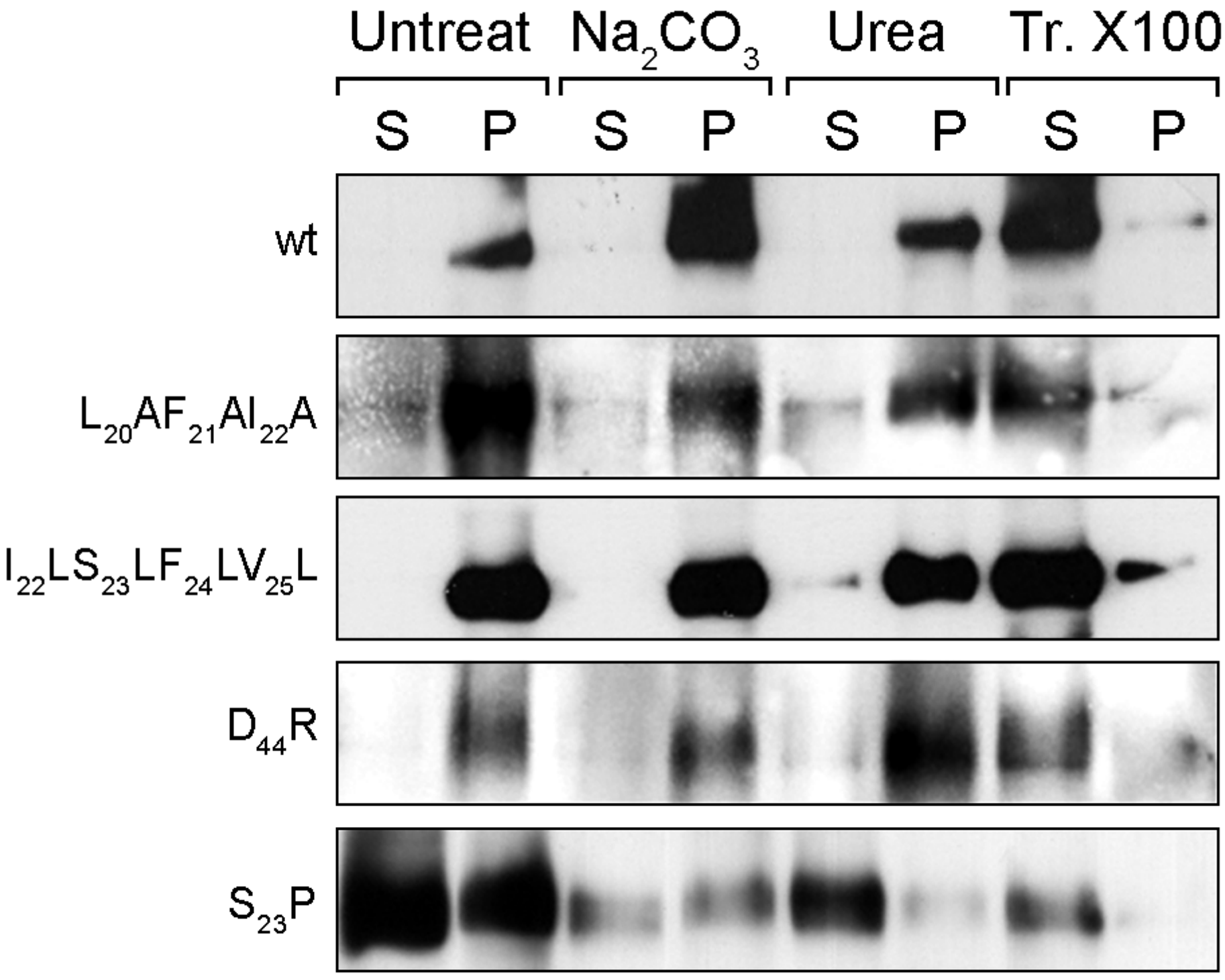
Untreat
Na_2CO_3
Urea
Tr. X100
S
P
S
P
S
P
S
P
wt
$L_{20}AF_{21}AI_{22}A$
$I_{22}LS_{23}LF_{24}LV_{25}L$
$D_{44}R$
$S_{23}P$

FIG. 3

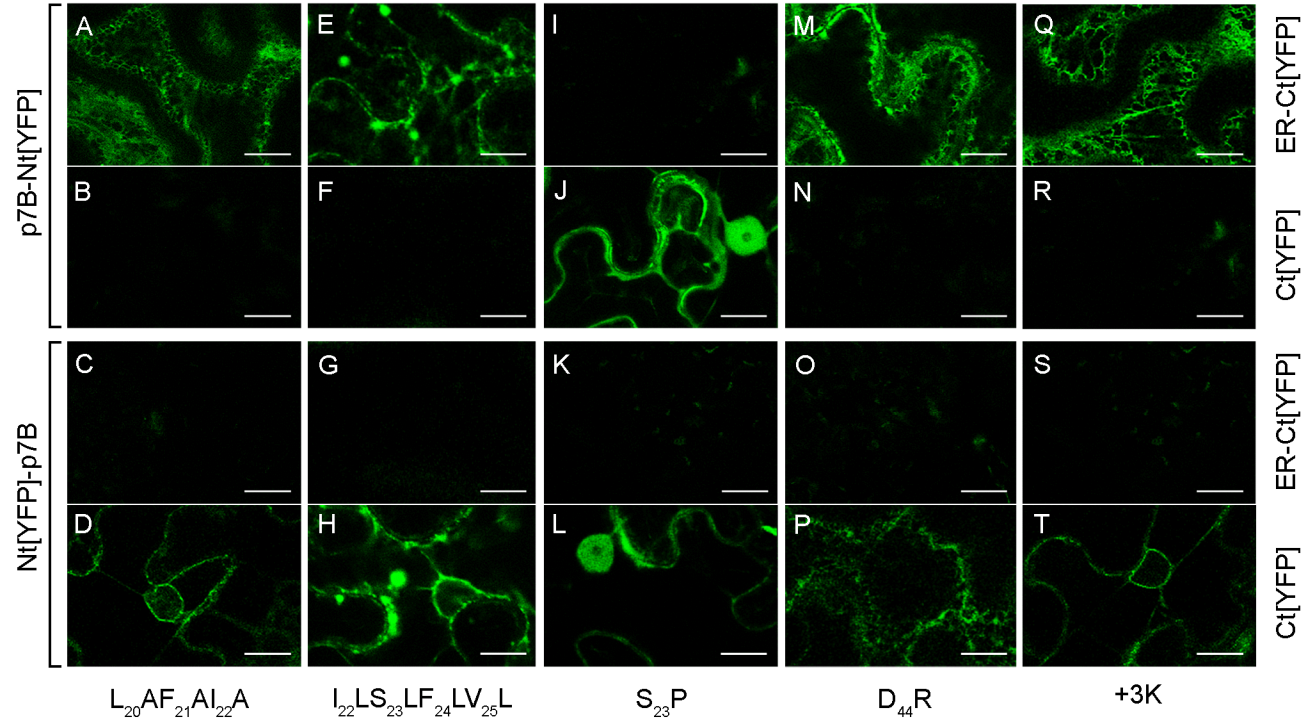
p7B-Nt[YFP]
Nt[YFP]-p7B
ER-Ct[YFP]
Ct[YFP]
ER-Ct[YFP]
Ct[YFP]
A
B
C
D
E
F
G
H
I
J
K
L
M
N
O
P
Q
R
S
T
L20AF21AI22A
I22LS23LF24LV25L
S23P
D44R
+3K

FIG. 4

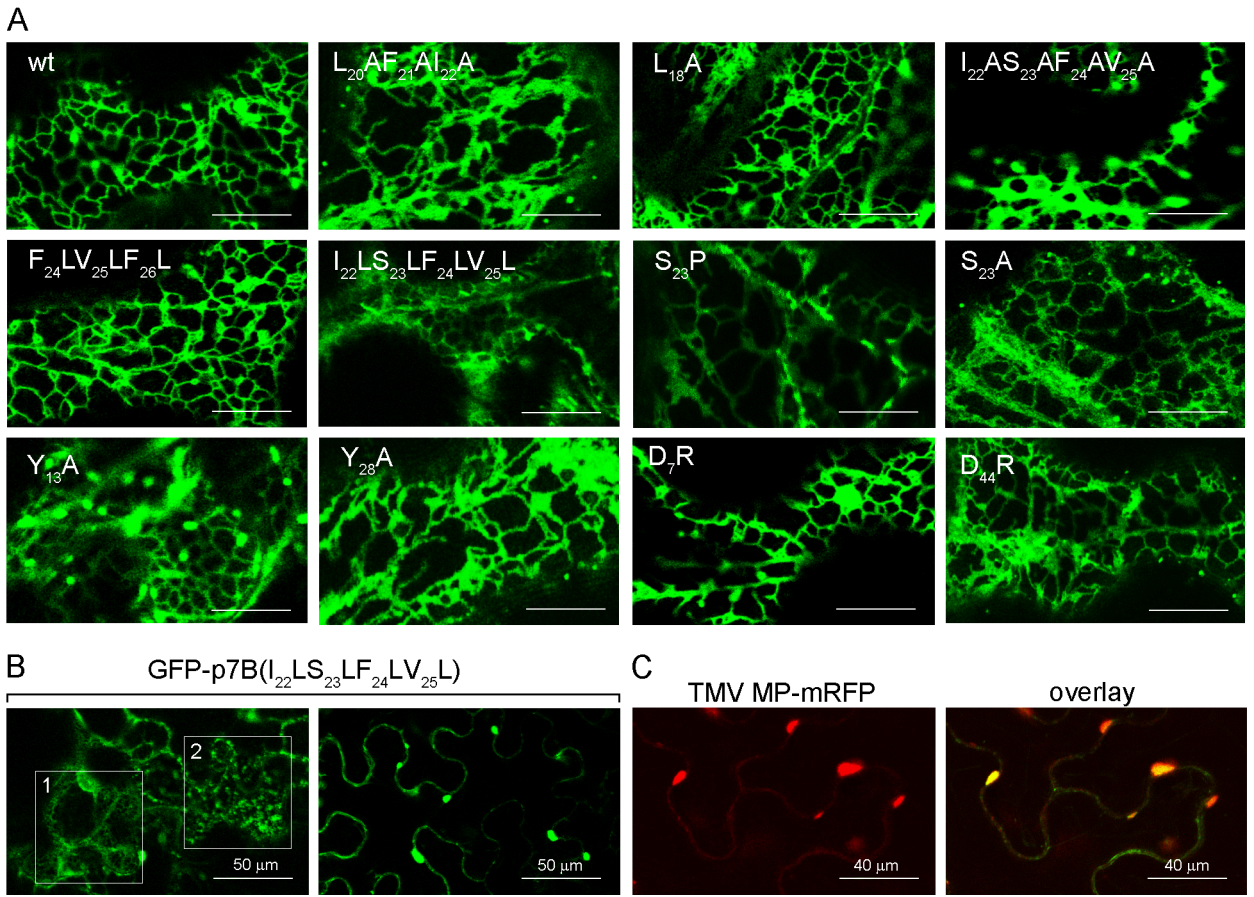
A
wt
L20AF21AI22A
L18A
I22AS23AF24AV25A
F24LV25LF26L
I22LS23LF24LV25L
S23P
S23A
Y13A
Y28A
D7R
D44R
B
GFP-p7B(I22LS23LF24LV25L)
1
2
50 µm
50 µm
C
TMV MP-mRFP
overlay
40 µm
40 µm

FIG. 5

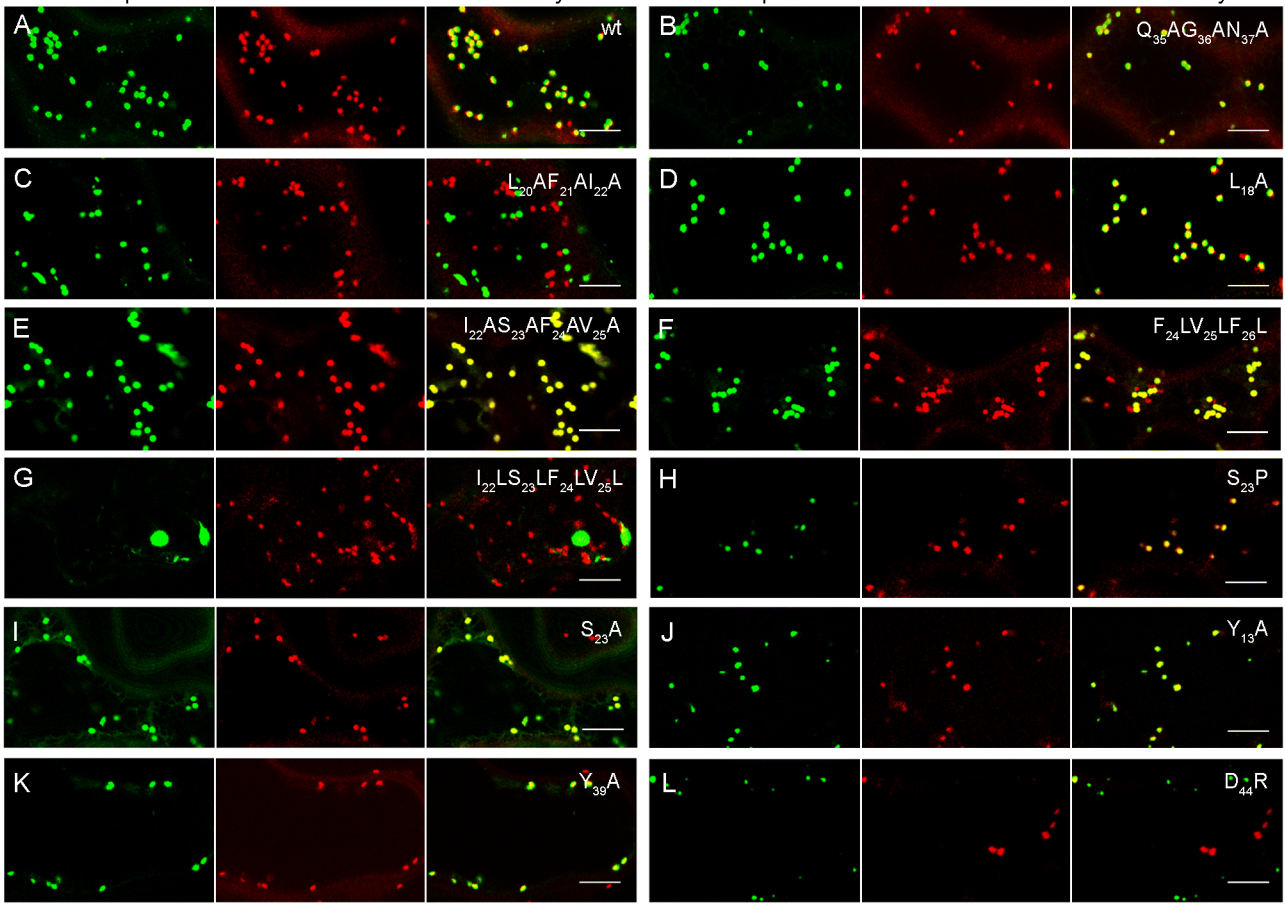
GFP-p7B
ChFP-STtmd
overlay
GFP-p7B
ChFP-STtmd
overlay
A
wt
B
$Q_{35}AG_{36}AN_{37}A$
C
$L_{20}AF_{21}AI_{22}A$
D
$L_{18}A$
E
$I_{22}AS_{23}AF_{24}AV_{25}A$
F
$F_{24}LV_{25}LF_{26}L$
G
$I_{22}LS_{23}LF_{24}LV_{25}L$
H
$S_{23}P$
I
$S_{23}A$
J
$Y_{13}A$
K
$Y_{39}A$
L
$D_{44}R$

FIG. 6

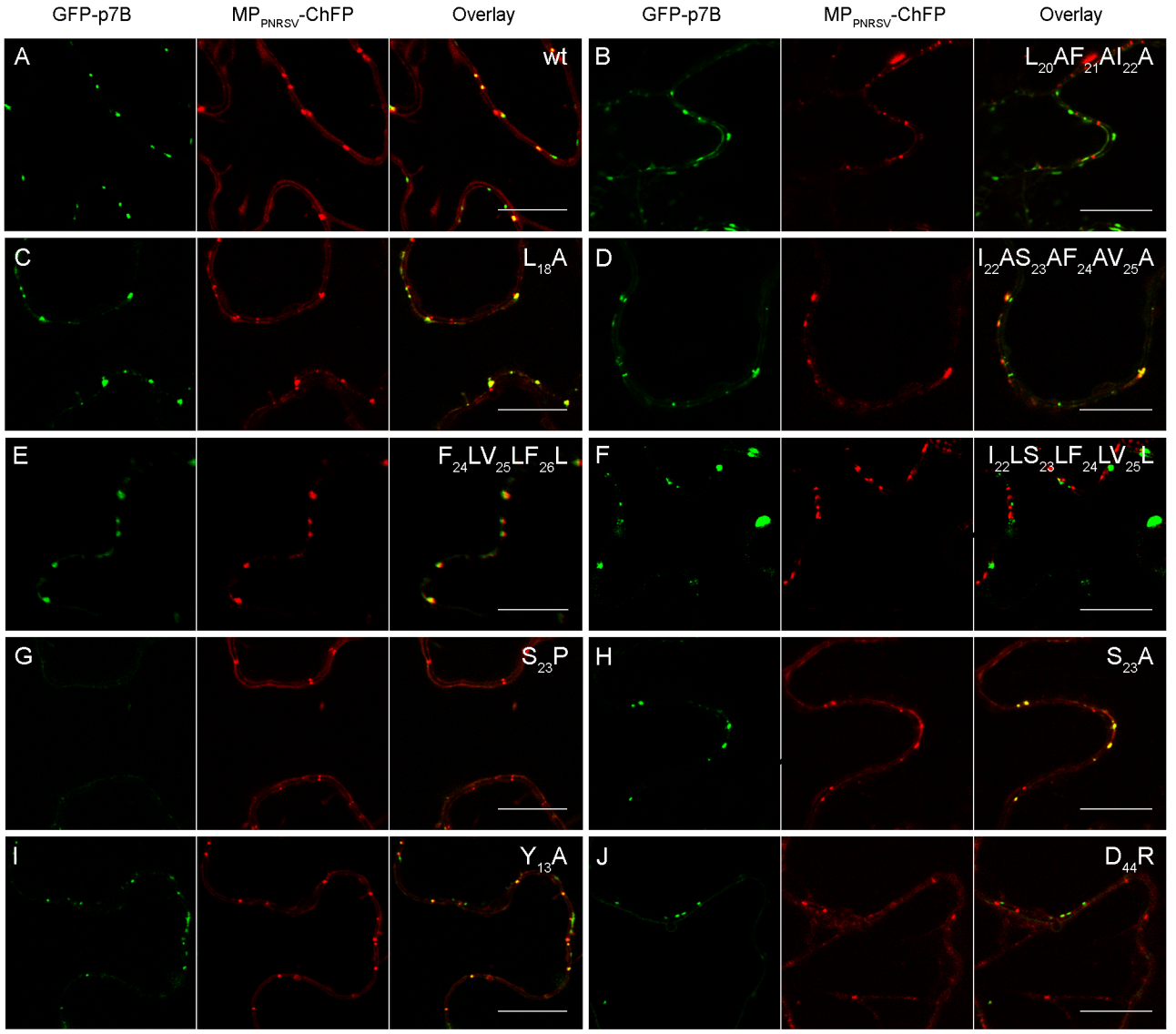
GFP-p7B
MP PNRSV-ChFP
Overlay
GFP-p7B
MP PNRSV-ChFP
Overlay
A
wt
B
L20AF21AI22A
C
L18A
D
I22AS23AF24AV25A
E
F24LV25LF26L
F
I22LS23LF24LV25L
G
S23P
H
S23A
I
Y13A
J
D44R

FIG. 7